DEEP LEARNING-BASED ANOMALY DETECTION IN NUCLEAR REACTOR CORES

Thanos Tasakos[1], George Ioannou[1], Vasudha Verma[2], Georgios Alexandridis[1], Abdelhamid Dokhane[2], and Andreas Stafylopatis[1]

[1]Institute of Communication and Computer Systems
National Technical University of Athens
Zografou, 157 80, Greece

[2]Paul Scherrer Institut
Laboratory for Reactor Physics and Thermal-Hydraulics
Forschungsstrasse 111, 5232 Villigen PSI, Switzerland

thanostas@islab.ntua.gr, geoioannou@islab.ntua.gr, vasudha.verma@psi.ch, gealexandri@islab.ntua.gr, abdelhamid.dokhane@psi.ch, andreas@cs.ntua.gr

dx.doi.org/10.13182/M&C21-33681

ABSTRACT

In this work, a methodology is proposed for the classification of different perturbation types and their position in a nuclear reactor core. More specifically, it is based on a Convolutional Neural Network architecture that identifies and locates specific perturbations, given the spectrograms of detector signals as input. Training samples have been provided by the SIMULATE-3K code, that simulates reactor core conditions. The different perturbation types considered are (i) realistic fuel assembly vibrations at different positions in the reactor core, (ii) fluctuations of inlet coolant temperature, (iii) fluctuations of inlet coolant flow and finally, (iv) combinations of the above sources. A complementary robustness analysis of the proposed architecture was performed to assess its performance in the cases of noisy or missing data. The trained model has subsequently been utilized on measurements obtained from the Gösgen Power Plant in Switzerland, for an assessment of its functionality.

KEYWORDS: neutron noise, anomaly detection, deep learning, convolutional neural networks, spectrograms, Simulate-3K, core diagnostics

1. INTRODUCTION

As the fleet of deployed Nuclear Power Plants (NPPs) in Europe and worldwide grows older, it becomes imperative to monitor their core conditions and take preemptive actions to ensure performance and safety [1]. One of the prevalent methods used for the assessment of the reactor core is noise diagnostics, that refer to the fluctuation of neutron flux around a mean value [2]. These signals are sampled from neutron detectors scarcely placed in the reactor core, and the main diagnostic task is to identify and locate the source of driving perturbations in the core based on the neutron flux captured at the detectors.

The current work employs machine learning techniques and more specifically, deep learning approaches, for perturbation identification & localization. Extending earlier work, a Convolutional Neural Network-based (CNN) architecture is presented, that models realistic perturbation types and their combinations, produced by the SIMULATE-3K code [3,4]. Section 2 reviews the relevant literature on the subject, while Section 3 describes the simulated data considered in this study. In Section 4, the proposed system is outlined and in Section 5 the training pipeline & the obtained results are demonstrated. Finally, the paper concludes in Section 6.

2. RELATED WORK

Machine Learning techniques have been widely applied to NPP data, both on simulated and actual plant measurements, for the assessment and diagnosis of the core state. Examples include symbolic dynamic filtering [5], that was used to down-sample input detector signals and then train a classifier. It has been demonstrated that this methodology performed better than principal component analysis, for simulated data produced by the International Reactor Innovative & Secure simulator. Support Vector Machines have also been considered for similar tasks; that is to assess the state of the reactor core [6] or for outlier identification on neutron flow signals originating from a nuclear reactor channel [7],

More recently, deep learning techniques have been utilized for noise diagnostics, as for example in [8], where a hybrid approach based on CNNs and denoising autoencoders, followed by k-means clustering, was proposed for perturbation identification and localization. Experiments performed on data generated by the CORE SIM [9] noise simulator exhibited promising results, even in the presence of (additive) noise to the signals, thereby validating its robustness. Additionally, a 3-dimensional CNN architecture for localizing perturbations has been presented in [10], based on frequency domain data. The same work also considers time-domain data (generated by the SIMULATE-3K code) that are provided as input to a Long Short-Term Memory (LSTM) network.

Finally, the wavelet transformation of detector signals is also used in conjunction with CNN architectures for efficient perturbation classification in [11]. In [12], an ensemble of Neural Networks has been proposed, consisting of one dimensional convolutions that extract the spatial characteristics of the detrended signals of neutron detectors, followed by LSTM layers that capture temporal features of the signals. Each neural network has been trained to recognize one specific perturbation type, with the experimental results demonstrating a satisfactory combined identification accuracy.

3. DESCRIPTION OF SIMULATED DATA

In this work, modeling of various noise sources based on realistic vibrations of fuel assemblies, fluctuations of thermal-hydraulic parameters of inlet coolant temperature and coolant flow, their combinations, and simulation of induced neutron noise are performed for the Swiss pre-KONVOI pressurized water reactor (PWR) [13]. It is a 3-loop reactor comprising of 177 fuel assemblies. The Paul Scherrer Institute (PSI) neutron noise methodology is based on the CASMO-5 (C5)/ SIMULATE-3 (S3) code system, coupled with the transient nodal code SIMULATE-3K (S3K) [14,15]. Vibrations of fuel assemblies are modeled with the so-called ‘delta-gap model’ in C5 that generates perturbed two-group macroscopic cross sections corresponding to varying water gap due to fuel assembly displacement. Post-processing of C5 nuclear data results in a readable binary-

formatted cross section library to be used by S3 and S3K for full core calculations. An external MATLAB script generates an include file containing time-wise delta-gap widths, that allows to simulate time-dependent fuel assembly vibrations with the "assembly vibration model" in S3K [16].

Table 1: Description of the transient scenarios along with the perturbation parameters

Case	Noise sources	Mode of vibration	Core condition	Vibration frequency	Maximum displacement	Relative perturbation from initial conditions
1.	Individual fuel assembly vibration	Cantilevered C-shaped S-shaped	BOC BOC BOC	1.2 Hz 1.2 Hz 5.0 Hz	1 mm 1 mm 1 mm	- - -
2.	Inlet coolant temperature fluctuations	- - -	BOC MOC EOC	- - -	- - -	$\pm 1^o$C $\pm 1^o$C $\pm 1^o$C
3.	Inlet coolant flow fluctuations	- - -	BOC MOC EOC	- - -	- - -	$\pm 2\%$ $\pm 2\%$ $\pm 2\%$
4.	Combination-I	Simplistic	BOC MOC EOC	1.2 Hz 1.2 Hz 1.2 Hz	1 mm 1 mm 1 mm	$\pm 1^o$C, $\pm 2\%$ $\pm 1^o$C, $\pm 2\%$ $\pm 1^o$C, $\pm 2\%$
5.	Combination-II	Cantilevered	BOC MOC EOC	1.2 Hz 1.2 Hz 1.2 Hz	1 mm 1 mm 1 mm	$\pm 1^o$C, $\pm 2\%$ $\pm 1^o$C, $\pm 2\%$ $\pm 1^o$C, $\pm 2\%$
6.	Combination-III	C-shaped	BOC MOC EOC	1.2 Hz 1.2 Hz 1.2 Hz	1 mm 1 mm 1 mm	$\pm 1^o$C, $\pm 2\%$ $\pm 1^o$C, $\pm 2\%$ $\pm 1^o$C, $\pm 2\%$
7.	Combination-IV	S-shaped	BOC MOC EOC	1.2 Hz 1.2 Hz 1.2 Hz	1 mm 1 mm 1 mm	$\pm 1^o$C, $\pm 2\%$ $\pm 1^o$C, $\pm 2\%$ $\pm 1^o$C, $\pm 2\%$

Having undergone improvements, the enhanced S3K version contains a module that enables the fuel assembly (FA) to vibrate in an axial pattern, representative of the vibration modes, by displacing each of the axial nodes by a certain width that is calculated using the user-assigned coefficients to each node and the water-gap widths at every time step. Models of in-core and ex-core neutron detectors are also included in the S3K input. The in-core detector model is composed of 36 detectors in total, distributed at 6 azimuthal locations and at 6 different axial levels. The ex-core detector model consists of 8 detectors in total, distributed at 4 azimuthal locations and at 2 axial levels. For a given set of operating conditions, S3K performs full core transient calculation to produce 3-D

two-group nodal neutron fluxes at each time step.

For the purpose of this study, detector responses obtained at the in-core neutron detector locations induced due to scenarios based on three main perturbation types and their combinations, are analyzed. The perturbation types are fuel assembly vibrations that include simplistic mode, cantilevered mode, C-shaped and S-shaped modes and inlet coolant flow & temperature fluctuations. The data is simulated at the Beginning-of-cycle (BOC), Middle-of-cycle (MOC) and End-of-cycle (EOC) of Cycle 40. The transient scenarios along with the perturbation parameters are given in Table 1. The simulations are performed for a duration of $100s$ at a time step of $0.01s$.

Note that in case 1, individual fuel assembly vibrations contain 177 scenarios each for every vibration mode, where each fuel assembly in the core is vibrated separately. Cases 4 – 7 representing combination scenarios contain simulations of central fuel assemblies in 5×5 clusters. All fuel assembly vibrations are performed in a synchronous pure-sinusoidal manner in the x-direction. All thermal-hydraulic perturbations of inlet coolant temperature and flow are introduced synchronously in all 3 loops of the PWR.

4. THE PROPOSED ARCHITECTURE

The core diagnostic task can be divided in two sub-tasks; the first one distinguishes the occurring perturbation type and the second one locates it in the reactor grid.

Figure 1 outlines the building blocks of the proposed neural network architecture for perturbation identification and localization. The input is a transformed version of the initial detector signals in the time domain, which are subsequently detrended and normalized. In order to collect more training examples the initial 100 sec simulations were split in multiple 10 sec windows. Then, the wavelet transformation of the signals is computed in order to represent them as *scaleograms* (the equivalent of the spectrogram of the Fourier transform), thereby obtaining a 2-dimensional representation of the signal. This encoding is subsequently provided as input to the convolutional layers of the network in order to extract spatial features that will help the model in the underlying task.

Example detector signal scaleograms are depicted in Figure 2, where the colorbar designates the power of a frequency at a specific timestamp, in logarithmic scale. Yellower colors represent increased power for the specific frequency, which aligns with the fact that the neutron noise signals have the majority of their power spectrum in low frequency ranges.

For the identification task, 4 different perturbation types are considered, pertaining to the 7 cases outlined in Table 1. More specifically, the studied perturbation types include 3 different modes of FA vibrations (Cantilevered, C-shaped & S-shaped) represented as one class and 2 thermal hydraulic fluctuations (inlet coolant temperature & flow) modeled separately. The last perturbation type considered is the combined case, where multiple perturbation types (FA vibration, thermal hydraulic fluctuations) co-occur in the rector grid. The reason for the separate modeling of the complex scenario was to help the network distinguish between simple perturbation scenarios and complex ones, in which the responses may be more complicated than a simple combination of the individual scenarios. Therefore, the binary output vector of the Identification Network (Figure 1) has a length of 4 bits, with ones designating the existence of a specific perturbation and zeros

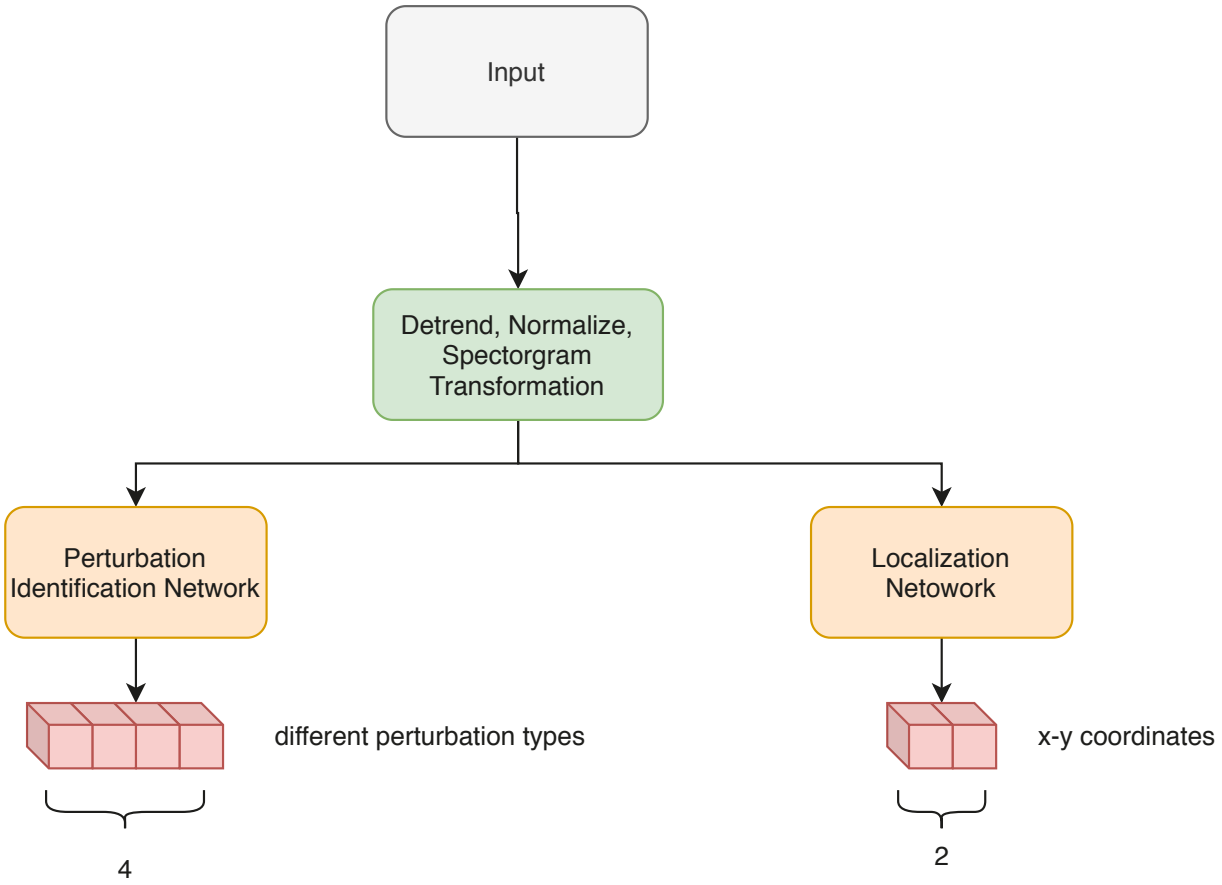

Figure 1: Proposed neural network architecture for perturbation identification and localization

indicating its absence, respectively.

For the localization task, the same architecture has also been employed. There exist 177 different perturbation sources (equal to the number of distinct fuel assemblies in the reactor core). In order to create a more general network, instead of modeling each different source as a separate class, the perturbation locations were encoded to x-y coordinates. The origin has been chosen to be at the center of the reactor grid. Therefore, the network outputs the point of the most prominent perturbation source.

Figure 3 displays the CNN architecture of the localization network (the structure of the identification network is similar; only the output layer is slightly different). The input (left) is a 44-channel image (one spectrogram for each in-core & ex-core detector), whose height and width are equal to the frequencies and the time window used, respectively. The image is subsequently processed and down-sampled by a number of successive convolutional blocks (in orange color), which actually perform the feature extraction process. Then, the extracted features are flattened into a vector and are provided to the fully connected component of the architecture (in purple color), along with an additional vector that holds information about the position of the detectors in the grid. Finally, the

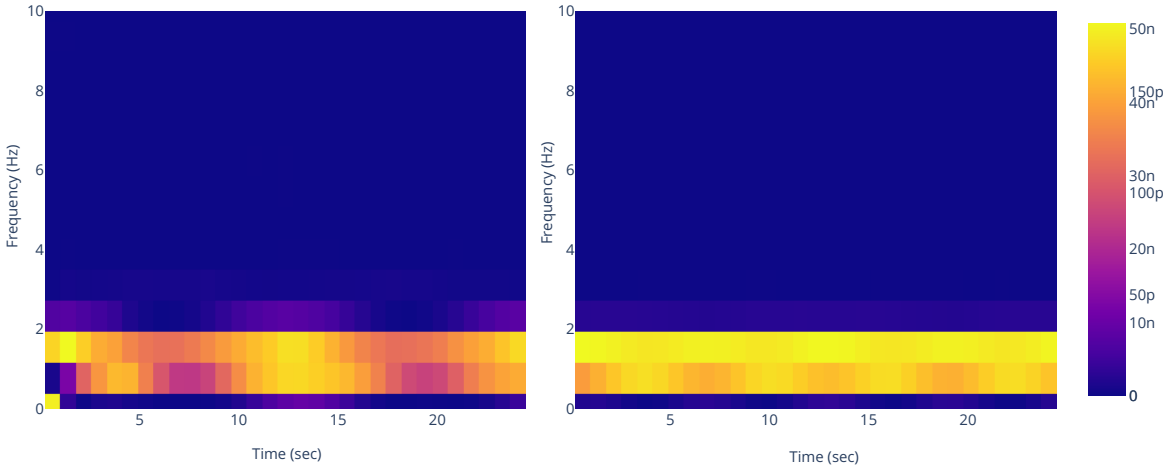

Figure 2: Example spectrogram input to the CNN architecture (the x, y axes represent time and frequency, respectively)

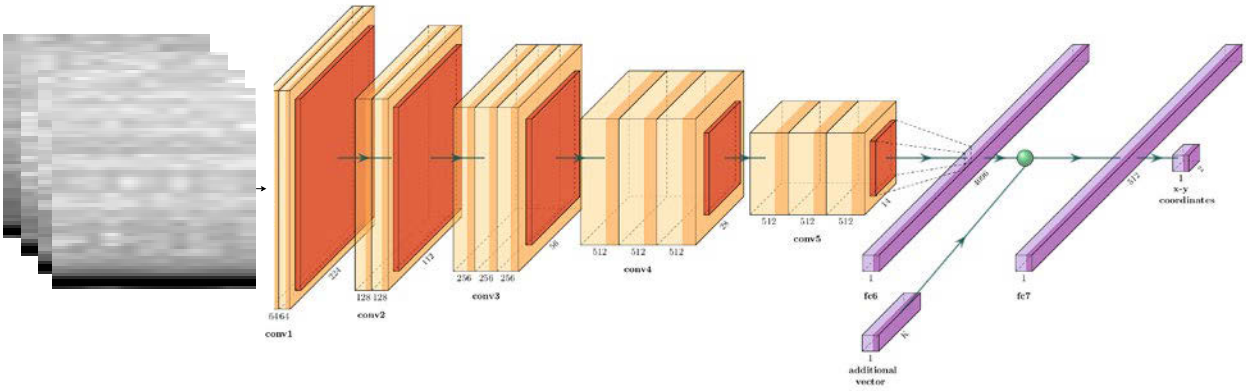

Figure 3: ResNet architecture for the localization task. Residual connections have been skipped for visual clarity.

network outputs the location of the vibrating vector (in x, y coordinates). Of course, the structure and hyper-parameters of the proposed architecture have been specified after thorough experimentation.

5. EXPERIMENTAL RESULTS

5.1. Perturbation identification task

Four different perturbation types have been given as input to the proposed model (FA vibration, inlet temperature & flow fluctuations and combined scenarios). In this task, the different modes of FA vibration (cantilevered, C-shaped and S-shaped) were treated as instances of the same perturbation type. In order to assess the robustness of the proposed architecture in the presence of external noise, input signals have been imputed with white noise of varying intensity, as measured by the signal-to-noise (SNR) ratio. Table 2 summarizes the performance of the identification network in terms of the *F1-score*, for varying noise levels.

Table 2: F1-score of the perturbation identification network for varying SNR ratios

Perturbation type	**SNR=**10	**SNR=**1	**SNR=**0.1	**SNR=**0.01
FA vibration	1.00	1.00	0.99	0.17
Inlet temperature fluctuation	1.00	0.99	0.53	0.30
Inlet flow fluctuation	1.00	1.00	0.62	0.09
Cluster vibration & thermohydraulical fluctuation	0.99	0.99	0.66	0.30

The F1-score is the harmonic mean of *Precision* and *Recall* and lies in the $[0, 1]$ range (higher values indicate better performance). Precision measures the ability of the system to correctly classify perturbations of a given type. It is equal to the ratio of correctly classified perturbations over all classified perturbations to the given type. Recall, on the other hand, measures the ability of the system to identify all perturbations belonging to a given type and is defined as the ratio of correctly classified perturbations to a given type over all perturbations actually belonging to that type.

The results of Table 2 indicate that the proposed architecture achieves optimal performance in identifying all perturbation types in the absence of noise (SNR=10) and even when the noise is a strong as the actual signal (SNR=0.1), thereby validating its robustness. As it is expected, when the noise becomes more powerful than the detector signal (SNR=0.1 and 0.01) the system's ability to distinguish between perturbation types deteriorates, but to a different degree for each of the examined cased (e.g. it seems to be deteriorating to a greater extend for the inlet temperature & flow fluctuations than the FA vibrations).

5.2. Localization task

As it has already been discussed, FA vibrations have been further studied, in an effort to identify the exact location (x, y coordinate) of the FA vibrating in the reactor core. A similar model to the perturbation identification network presented above has been trained to output the location of the vibrating FA. The loss function used is the mean square error between the actual and the predicted

coordinates of the vibrating FA, as it measures how close the predictions to their real counterparts really are.

Table 3: Prediction accuracy of the localization network

Prediction proximity	Proportion of the test set
exact	0.73
1 difference	0.21
> 1 difference	0.06

Table 3 summarizes the prediction accuracy of the localization network. In 73% of all cases, the system is able to identify the exact vibrating FA. In another 21% of the cases, the system is able to identify a neighboring FA, while in only 6% of all cases the prediction is not in the immediate neighborhood of the vibrating FA. From the presented results, it can be deduced that the localization network is extremely accurate.

5.3. Faulty detectors

A complementary robustness analysis regarding faulty detectors has also been performed on the proposed system. The purpose of the study is to assess the distinguishing capability of the models, given partial information about the grid condition. This is especially crucial because the existence of faulty detectors is not uncommon in NPP operation. In order to emulate this situation in the current task, 6 different subsets of either in-core or in-core & ex-core detectors have been considered. Their location on the grid is depicted in Figure 4, while their combinations are summarized in the top two rows of Table 4.

Table 4: Prediction accuracy of the localization network for different subsets of functional detector signals

	Functional subsets of detectors					
Prediction proximity	I_1, I_2, I_5	I_1, I_2, I_5 + ex-core	I_3, I_4, I_6	I_3, I_4, I_6 + ex-core	I_1, I_3, I_4	I_1, I_3, I_4 + ex-core
exact	0.52	0.58	0.48	0.65	0.43	0.66
1 difference	0.31	0.32	0.32	0.26	0.34	0.22
2 difference	0.11	0.07	0.13	0.07	0.15	0.09
> 2 difference	0.06	0.03	0.07	0.02	0.08	0.03

The prediction accuracy of the subsets of functional detector signals is displayed on Table 4. As it is expected, the performance of all functional subsets of detectors is inferior when compared to the case of all working detectors (Table 3). Nevertheless, it can be argued that in most cases, it is

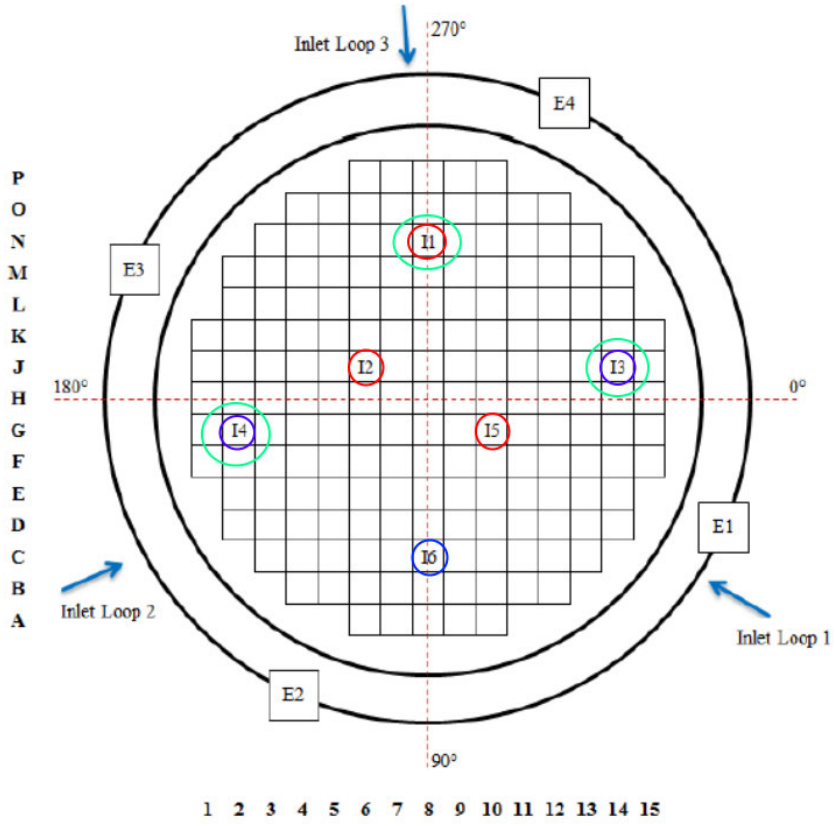

Figure 4: Position of the detectors on the grid

still possible to either identify the exact vibrating FA or its direct neighborhood with an accuracy ranging from 60% to 80%. Additionally, the presence of the ex-core detectors in all cases improves the results, as a higher number of detectors uniformly within and around the core likely helps in improving diagnostics of the core. Out of those results, two main conclusions may be drawn: (i) better coverage of the reactor grid leads to better localization accuracy and (ii) the model is robust enough, even when smaller detector subsets are considered.

5.4. Preliminary comparison with plant measurements

In principle, the first layers of a deep neural network architecture act as feature extractors for the data the network is trained upon. Therefore, if the simulated data constitute a good representation of the actual plant measurements, then the feature extraction procedure may be applied to the actual plant measurements as well, leading to possible perturbation identification and localization in the operating NPP. Based on this observation, data obtained during BOC 40 of the Gösgen Power Plant in Switzerland [17] (3-loop pre-KONVOI reactor) have been provided to the system trained on simulated data.

In order to match plant measurements to simulated signals, a series of pre-processing steps were

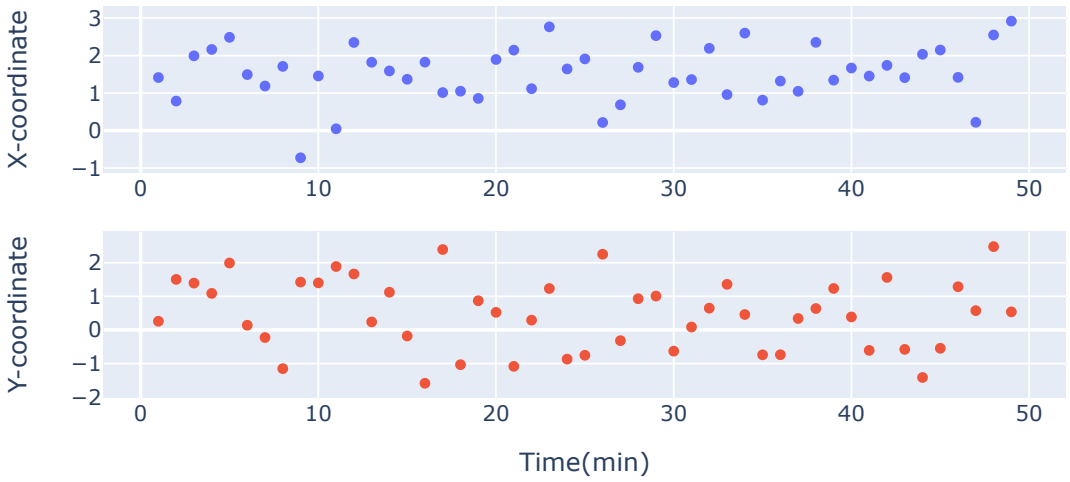

Figure 5: Predictions of the x-y coordinates of perturbations on plant data

necessary. Firstly, re-sampling has been performed in order to mach the measurements' sampling rate to the simulated data. Additionally, because the duration of the plant measurements were 50 minutes, while the simulated signals last for 100 seconds, samples of 10 seconds were drawn from the plant measurements every minute, resulting in a total of 50 data points.

Figure 5 depicts the predictions of the perturbation localization network for FA vibrations. Those seem to oscillate around the reactor center ($x = 0, y = 0$ represent the centre of the core, radially), mainly to the positive direction of the x (1^{st} and 4^{th} quartiles). The mean predicted vibrating FA is located at $(1.5, 0.5)$, with $\sigma_x = 0.73, \sigma_y = 1.05$. These results predominately locate single vibrating FAs near the center of the core (radially); nevertheless they are not necessarily indicative of inferior performance of the proposed methodology on plant measurements, because it could also be possible that this specific perturbation type (single vibrating FA) is not present in the reactor.

6. CONCLUSIONS

A noise diagnostics pipeline for automatic identification and localization of perturbation sources based on CNNs has been proposed in this work. Initial results exhibit satisfactory distinguishing capability on simulated data. A complimentary robustness analysis has been performed, exhibiting the applicability of the proposed architecture to smaller subsets of detectors. The trained model has been subsequently tested on actual measurements from a NPP in order to draw insights regarding possible underlying perturbations. Further investigation is necessary to assess its distinguishing capability on real plant measurements.

ACKNOWLEDGEMENTS

The research conducted has been made possible through funding from the Euratom research and training programme 2014-2018 under grant agreement No 754316 for the "CORe Monitoring Techniques And EXperimental Validation And Demonstration (CORTEX)" Horizon 2020 project, 2017-2021. Additionally, the authors would like to thank Kernkraftwerk Gösgen-Däniken AG and Institut fuer Sicherheitstechnologie GmbH for the provided actual plant measurements.

REFERENCES

[1] J. Ma and J. Jiang. "Applications of fault detection and diagnosis methods in nuclear power plants: A review." *Progress in Nuclear Energy*, **volume 53**(3), pp. 255 – 266 (2011). URL http://www.sciencedirect.com/science/article/pii/S0149197010001769.

[2] I. Pázsit and C. Demazière. *Noise Techniques in Nuclear Systems*, pp. 1629–1737. Springer US, Boston, MA (2010). URL https://doi.org/10.1007/978-0-387-98149-9_14.

[3] G. Grandi. "SIMULATE-3K Input specification (SSP-98/12, Rev. 17)." (2015).

[4] D. Chionis, A. Dokhane, L. Belblidia, M. Pecchia, G. Girardin, H. Ferroukhi, and A. Pautz. "SIMULATE-3K analyses of neutron noise response to fuel assembly vibrations and thermal-hydraulics parameters fluctuations." In *M&C 2017-International Conference on Mathematics & Computational Methods Applied to Nuclear Science & Engineering, at Jeju, Korea* (2017).

[5] X. Jin, Y. Guo, S. Sarkar, A. Ray, and R. M. Edwards. "Anomaly Detection in Nuclear Power Plants via Symbolic Dynamic Filtering." *IEEE Transactions on Nuclear Science*, **volume 58**(1), pp. 277–288 (2011).

[6] N. Zavaljevski and K. C. Gross. "Support vector machines for nuclear reactor state estimation." Technical report, Argonne National Lab. (2000).

[7] C. K. Maurya and D. Toshniwal. "Anomaly detection in nuclear power plant data using support vector data description." In *Proceedings of the 2014 IEEE Students' Technology Symposium*, pp. 82–86. IEEE (2014).

[8] F. Caliva, F. S. De Ribeiro, A. Mylonakis, C. Demaziere, P. Vinai, G. Leontidis, and S. Kollias. "A deep learning approach to anomaly detection in nuclear reactors." In *2018 International Joint Conference on Neural Networks (IJCNN)*, pp. 1–8. IEEE (2018).

[9] C. Demaziere. "CORE SIM: A multi-purpose neutronic tool for research and education." *Annals of Nuclear Energy*, **volume 38**(12), pp. 2698–2718 (2011).

[10] A. Durrant, G. Leontidis, and S. Kollias. "3D convolutional and recurrent neural networks for reactor perturbation unfolding and anomaly detection." *EPJ Nuclear Sciences & Technologies* (2019).

[11] T. Tagaris, G. Ioannou, M. Sdraka, G. Alexandridis, and A. Stafylopatis. "Putting Together Wavelet-Based Scaleograms and Convolutional Neural Networks for Anomaly Detection in Nuclear Reactors." In *Proceedings of the 2019 3rd International Conference on Advances in Artificial Intelligence*, ICAAI 2019, p. 237–243. Association for Computing Machinery, New York, NY, USA (2019). URL https://doi.org/10.1145/3369114.3369121.

[12] G. Ioannou, T. Tagaris, G. Alexandridis, and A. Stafylopatis. "Intelligent Techniques for Anomaly Detection in Nuclear Reactors." (2020).

[13] R. Ferrer. "CASMO-5 Methodology Manual." Technical report, (SSP-08/405 - Rev 4) (2015).

[14] G. Grandi. "SIMULATE-3K Models & Methodology." Technical report, (SSP-98/13 Rev. 7) (2011).

[15] U. P. J. Pohlus J and G. Girardin. "Report about the measurement results of Goesgen." Technical report, CORTEX deliverable D4.1 (2018).

[16] D. Chionis, A. Dokhane, L. Belblidia, H. Ferroukhi, G. Girardin, and A. Pautz. "Development and verification of a methodology for neutron noise response to fuel assembly vibrations." *Annals of Nuclear Energy*, **volume 147**, p. 107669 (2020). URL http://www.sciencedirect.com/science/article/pii/S0306454920303674.

[17] S. Lipcsei, S. Kiss, J. Pohlus, U. Paquee, G. Girardin, C. Pohl, M. Seidl, P. Stulik, M. Bem, J. Machek, B. Shumaker, and E. Riggsbee. "CORTEX Deliverable 4.3: Document describing all validation data." deliverable D4.3, Core monitoring techniques and experimental validation and demonstration (CORTEX), Horizon 2020 EU Framework Programm (No. 754316) (2018).